

# Fabrication of diffraction gratings for hard X-ray phase contrast imaging

C. David <sup>\*</sup>, J. Bruder, T. Rohbeck, C. Grünzweig, C. Kottler, A. Diaz, O. Bunk, F. Pfeiffer

*Paul Scherrer Institut, CH 5232 Villigen-PSI, Switzerland*

Available online 2 February 2007

## Abstract

We have developed a method for X-ray phase contrast imaging, which is based on a grating interferometer. The technique is capable of recording the phase shift of hard X-rays travelling through a sample, which greatly enhances the contrast of low absorbing specimen compared to conventional amplitude contrast images. Unlike other existing X-ray phase contrast imaging methods, the grating interferometer also works with incoherent radiation from a standard X-ray tube. The key components are three gratings with silicon and gold structures, which have dimensions in the micrometer range and high aspect ratios. The fabrication processes, which involve photolithography, anisotropic wet etching, and electroplating, are described in this article for each of the three gratings. An example of an X-ray phase contrast image acquired with the grating interferometer is given.

© 2007 Elsevier B.V. All rights reserved.

*Keywords:* Radiography; Medical imaging; Anisotropic silicon wet etching; Gold electroplating

## 1. Introduction

X-ray radiographic imaging is an invaluable tool to investigate the inner structure of thick samples. The most important applications are medical imaging and the inspection of products on production lines or luggage on airports. The contrast mechanism presently used in such imaging systems is based on the differences in absorption of the samples constituents. However, for biological tissue samples, polymers or fibre composites, the use of conventional X-ray radiography is limited due to their weak absorption. By recording the phase shift of the X-rays passing through the sample instead of the absorption, the contrast of radiographs can be greatly enhanced. A number of techniques have been developed in the past years to exploit X-ray phase contrast [1,2], but as they all need a considerable degree of coherence of the used radiation, none of them can be used with the incoherent radiation of standard X-ray tube sources. This is the reason why they have not

found any wide spread application in hospitals, factories, or airports.

We have recently developed an interferometric X-ray phase contrast imaging method based on diffraction gratings [3,4]. The great advantage of the method is the fact that it can be used with the polychromatic spectrum of an incoherent X-ray tube [5]. The principle of the method is based on detecting minute changes in the direction of propagation, which are caused by refraction of the X-rays passing through a phase shifting object. Equivalent to refraction in the visible range, the change in direction is proportional to the local gradient in phase shift, however, it should be noted, that the refractive power of matter for X-rays is many orders of magnitude weaker. The principle of the experimental set-up is shown in Fig. 1. The essential part of the interferometer consists of two gratings placed between the object and the image detector, which act as an array of collimating slits that have a transmission depending strongly on the relative position of the two gratings and the angle of incidence. Thus, any local phase gradient in the object causes a local change in intensity recorded on the detector. While the analyzer grating close

<sup>\*</sup> Corresponding author. Tel.: +41 56 310 3753.

E-mail address: [christian.david@psi.ch](mailto:christian.david@psi.ch) (C. David).

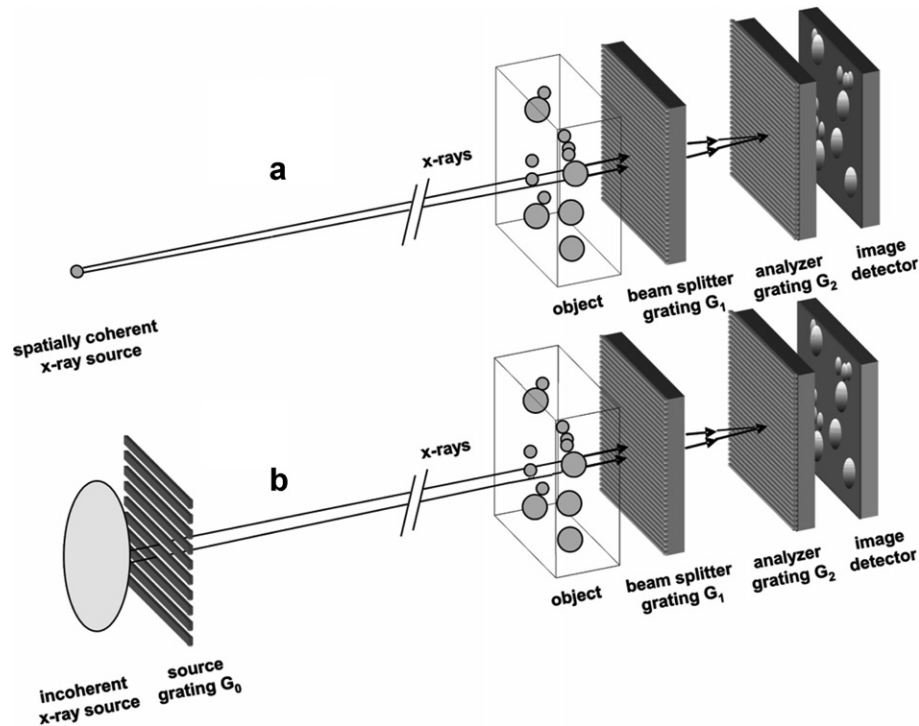


Fig. 1. Schematic view of the grating-based X-ray interferometer for phase contrast imaging. The two-grating set-up (a) is used with spatially coherent radiation such as synchrotron radiation, whereas the three-grating set-up (b) can be used with incoherent radiation from a standard X-ray tube.

to the detector consists of an array of highly absorbing gold lines, the beam splitter grating just downstream of the object is made of phase shifting lines, which reduces the losses of the set-up. Note that the described set-up does not require monochromatic radiation. More details on the optical considerations and the data acquisition procedure can be found elsewhere [4].

It is evident, that such a set-up with only two gratings (as shown in Fig. 1a) requires a source that provides sufficient spatial coherence, i.e., which is small enough and far away enough to provide a sufficiently narrow angular uncertainty of the incoming rays. Whereas this is not a problem at a synchrotron, where the source is usually less than a millimeter in size and situated tens of meters away from the experiment, this poses a severe restriction for the use in laboratory equipment based on X-ray tubes, which usually cannot be placed at sufficiently large distances for reasons of required compactness and flux density. This problem can be solved by introducing a third grating just downstream of the source (see also Fig. 1b), that essentially creates an array of spatially coherent line sources. If the condition  $p_0 = p_2 \times l/d$  is fulfilled, where  $p_0$  and  $p_2$  are the periods of the source grating and the analyzer grating,  $l$  is the source grating to beam-splitter grating distance and  $d$  is the beam-splitter grating to analyzer grating distance, then the images created by each line source are superimposed in the image plane. The implementation of such a source grating therefore makes it possible to use incoherent radiation sources, resulting in an efficient use of the available flux.

## 2. Grating fabrication

For each of the three gratings, a different fabrication process was chosen, as the dimensions and X-ray optical requirements are quite different. The source grating  $G_0$  is fairly easy to make, as its period  $p_0$  is typically on the order 15–150  $\mu\text{m}$ . Moreover, the total area of  $G_0$  only needs to be large enough to cover the source size, i.e., a few square millimetres are sufficient. The main requirement of the grating structures is a sufficient height of the gold absorber. In our present setup, we use X-ray photon energies up to 30 keV. It can be calculated from the X-ray optical constants of gold [6], that 40  $\mu\text{m}$  thickness corresponds to a transmission of only a few percent. We use a standard photo lithography process for the pattern definition (see Fig. 2, left). The samples are coated with a thin plating base of 15 nm of titanium and 50 nm of silver. A 50  $\mu\text{m}$  layer of SU8 resist (XP KMPR 1050 by Kayaku MicroChem Ltd.) is spin-coated on to the plating base. After exposure and development, the gold structures with heights of 40–45  $\mu\text{m}$  are plated onto the sample from a cyanide based plating bath (Autronex CC-AF-B by Enthone Omi) using a current density of 3.5 mA/cm<sup>2</sup>. After the deposition, the SU8 resist can be stripped in *N*-methyl-2-pyrrolidone (NMP) even though this is not required with respect to the optical performance, as the resist is transparent to X-rays. A scanning electron micrograph of the resulting structures is shown in the right part of Fig. 2.

The requirements for the beam splitter grating  $G_1$  are more challenging. It should consist of low absorbing,

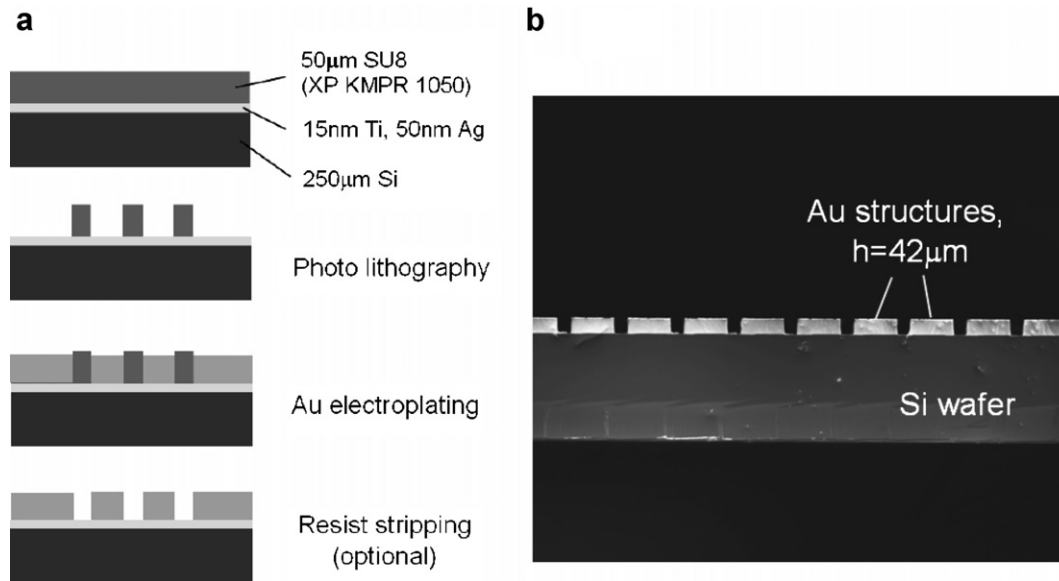


Fig. 2. Left: fabrication process used to make the source grating  $G_0$ . Right: cross section of a source grating with  $127 \mu\text{m}$  period and a gold absorber thickness of  $42 \mu\text{m}$ . The SU8 resist has been removed in NMP solution. The silicon wafer thickness is  $250 \mu\text{m}$ .

phase shifting structures with a period  $p_1 \sim 4 \mu\text{m}$ . The best performance is achieved when the structures have a duty cycle of 0.5, and the height is chosen such that they introduce a phase shift of  $\pi$ . Furthermore, the grating area limits the field of view of the imaging device, so it should be many centimetres in size, depending on the application. We chose  $100 \text{ mm}$   $\langle 110 \rangle$  oriented silicon wafers,  $280 \mu\text{m}$  thick, both sides polished, as substrates. The wafer size limits the area of our gratings to  $64 \text{ mm} \times 64 \text{ mm}$ . The grating fabrication process is depicted in the left part of Fig. 3. The grating structures are etched into the silicon substrates. First, the photo resist pattern is transferred

into a thin oxide layer which then serves as a mask for the anisotropic wet etching process in 20% aqueous KOH solution. At  $76^\circ\text{C}$ , we obtained an etch rate of  $1.68 \mu\text{m}/\text{min}$  in the  $\langle 110 \rangle$  direction. The etch rate along the  $\langle 111 \rangle$  directions is about  $80\times$  slower, resulting in nearly perpendicular side walls of the structures. This is confirmed by an inspection of the structures. The right part of Fig. 3 shows a cross section of a beam splitter grating with a structure height of  $22 \mu\text{m}$ , which corresponds to a  $\pi$ -phase shift for  $17.5 \text{ keV}$  photon energy. The oxide masking layer has been removed in buffered oxide etch (BOE) before inspection.

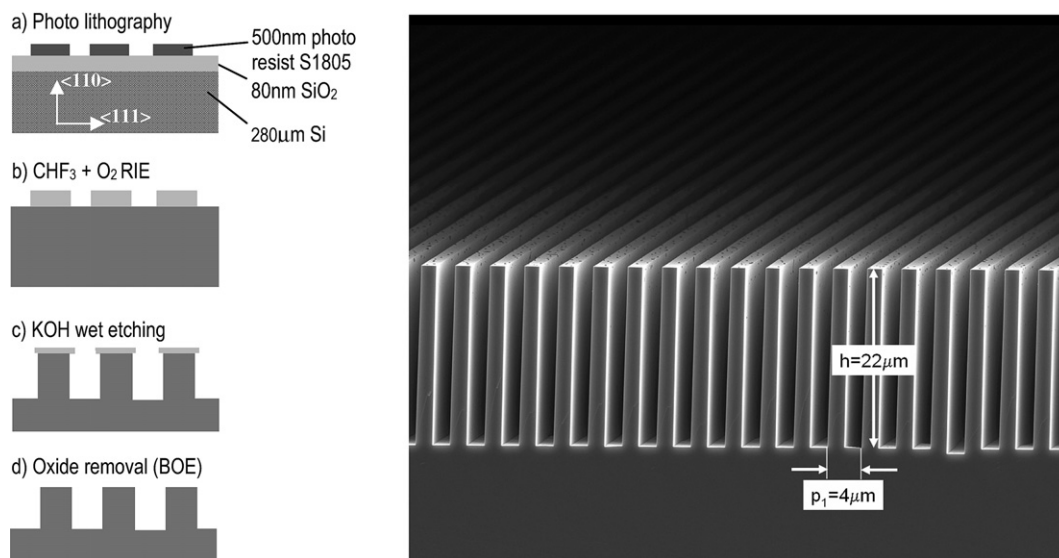


Fig. 3. Left: fabrication process for the beam splitter grating  $G_1$ . The  $\langle 110 \rangle$  silicon substrate is anisotropically etched in a KOH solution resulting in high aspect ratio structures with nearly vertical side walls. Right: cross section of a  $4 \mu\text{m}$  period grating with a structure height optimized for  $17.5 \text{ keV}$  photon energy.

The fabrication of the analyzer grating  $G_2$  is the most challenging part, as the grating period is only  $p_2 = 2 \mu\text{m}$ , and large areas have to be patterned with good uniformity. The required thickness of the gold absorber structures should be sufficient to provide a high contrast. A transmission of the structures of less than 25% is acceptable. It can be calculated [6], that  $10 \mu\text{m}$  thickness is sufficient for photon energies below 20 keV. For photon energies of 30 keV, about  $25 \mu\text{m}$  of gold is required. We pursue two approaches for the fabrication of high aspect ratio gratings

on 100 mm wafers with areas of up to  $64 \text{ mm} \times 64 \text{ mm}$ . The first method is shown in the upper part of Fig. 4. A silicon grating with a period of  $2 \mu\text{m}$  and a duty cycle of 0.5 is used as substrate, and the grating grooves are filled with gold by electroplating. It is essential that the filling starts only at the bottom of the grooves to ensure a complete, uniform filling. For this purpose, a  $200 \text{ nm}$  thick sacrificial layer of aluminium is evaporated under a sloped angle with respect to the grating structures. Then the plating base consisting of a  $15 \text{ nm}$  thick adhesive layer of chromium and a

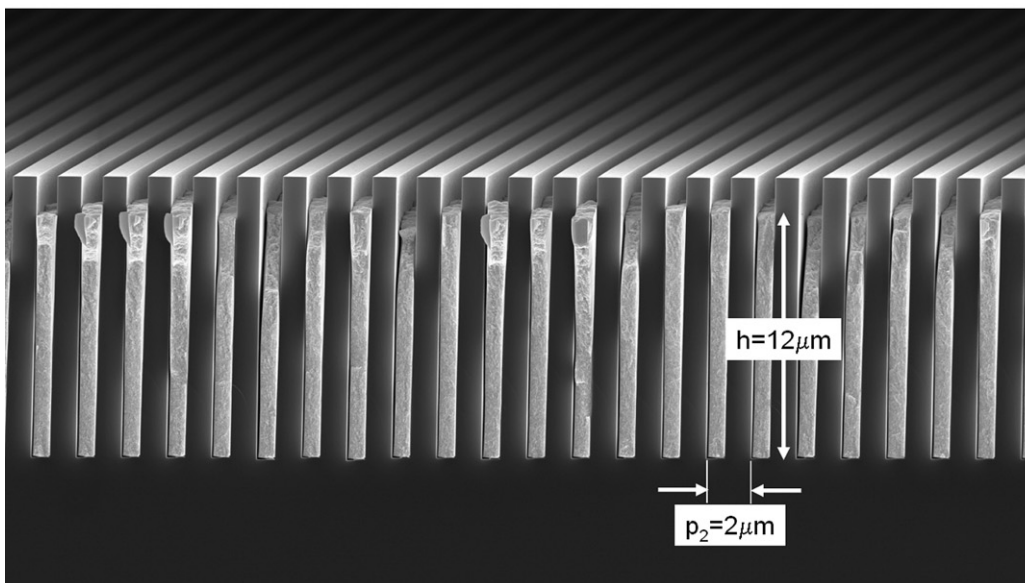
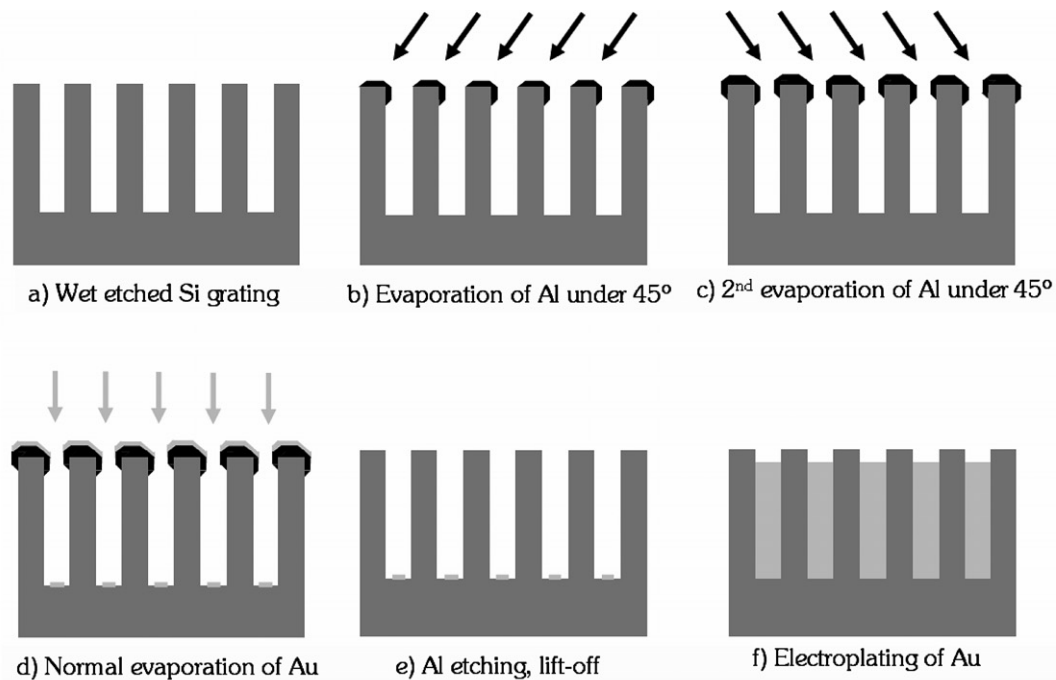


Fig. 4. Top: fabrication steps to make the analyzer grating  $G_2$ . A silicon grating is metallised with an Al sacrificial layer and a gold plating base, so that the grooves of the grating can be selectively filled with gold by electroplating. Bottom: cross section of an analyzer grating with  $2 \mu\text{m}$  period and  $12 \mu\text{m}$  high absorber structures.

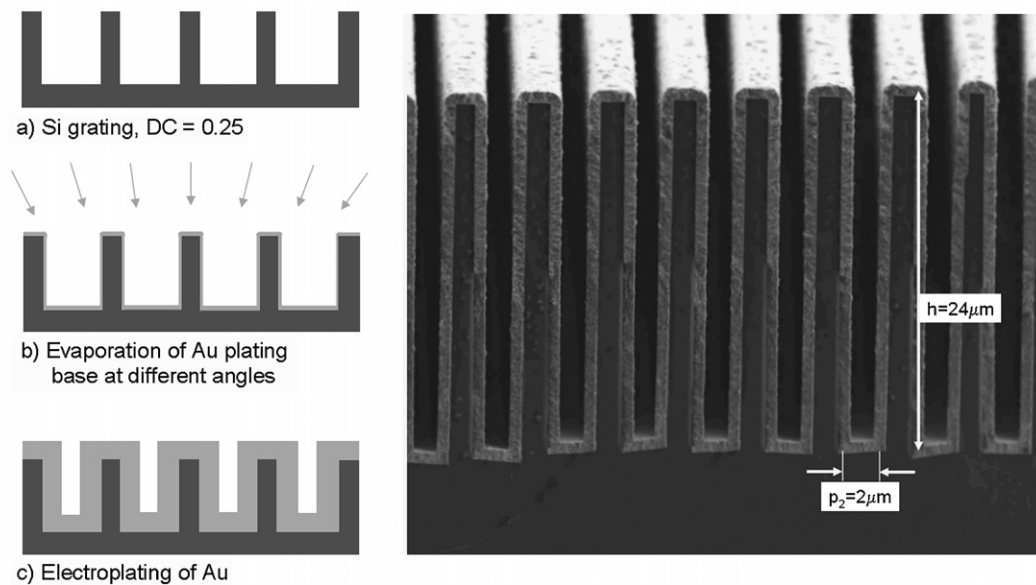


Fig. 5. Left: fabrication steps used to produce analyzer gratings with very high aspect ratio absorber structures. A silicon grating with a duty cycle of 0.25 is coated with a homogeneous gold layer. Right: cross section of an analyzer grating with an effective period of  $2\ \mu\text{m}$  and an aspect ratio of 24.

50 nm thick layer of gold is evaporated onto the sample under normal incidence. By etching away the aluminium in phosphoric acid, the gold is removed from the ridges of the grating lines, whereas the plating base remains on the bottom of the grooves. The same plating bath was used as for the fabrication of the source grating  $G_0$ , the current density was again set to  $3.5\ \text{mA}/\text{cm}^2$ . This procedure was successful for the fabrication of structures with aspect ratios up to 12, i.e., up to a structure height of up to  $12\ \mu\text{m}$ . The lower part of Fig. 4 shows the cross section of an analyzer grating. For higher aspect ratios, the deposition of the plating base in the grooves of the silicon grating becomes more and more difficult, as some of the metal is deposited on the side walls. This results in an inhomogeneous, incomplete filling of the structures.

To obtain structures with even higher aspect ratios, the method depicted in the left part of Fig. 5 was developed. The basis of the process is a silicon grating, again produced by anisotropic wet etching, which has a period of  $4\ \mu\text{m}$  and a duty cycle of 0.25. A  $15\ \text{nm}$  thick adhesive layer of chromium and a  $50\ \text{nm}$  thick layer of gold were evaporated onto the grating. During the evaporation, the grating is tilted by several degrees to assure that some of the metal is also covering the side walls of the silicon structures. The grating structures were then covered with a  $1\ \mu\text{m}$  thick layer of gold by electroplating. Due to the high aspect ratio of the silicon structures, most of the gold is deposited onto the side walls resulting in absorber structures with an effective period of  $2\ \mu\text{m}$ . The high aspect ratio of the structures inhibits a fast exchange of electrolyte solution, which leads to a depletion of the electrolyte solution for high current densities. In order to obtain a homogenous coverage of the structures, it turned out to be necessary to reduce the

current density to only  $0.2\ \text{mA}/\text{cm}^2$ . The right part of Fig. 5 shows a grating with  $24\ \mu\text{m}$  high gold structures, which provide sufficient contrast even for  $30\ \text{keV}$  photon energy.

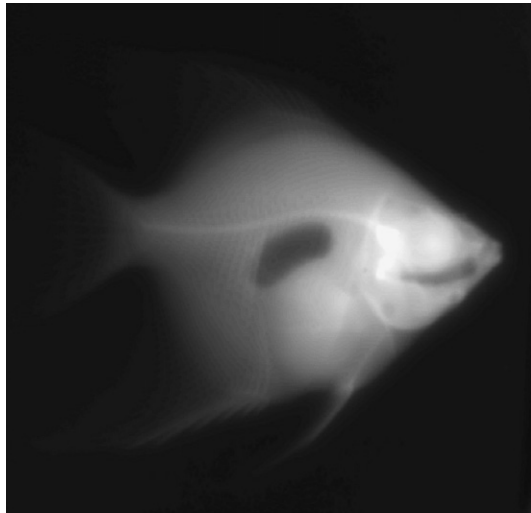
The main advantages of this method compared to the one described in Fig. 4 are the bigger structure periods that need to be made by photolithography, and the higher aspect ratios that can be achieved. However, the control of the duty cycle and the plated layer thickness is more critical in the latter process, as both have a direct effect on the position of the gold structures.

### 3. X-ray imaging results

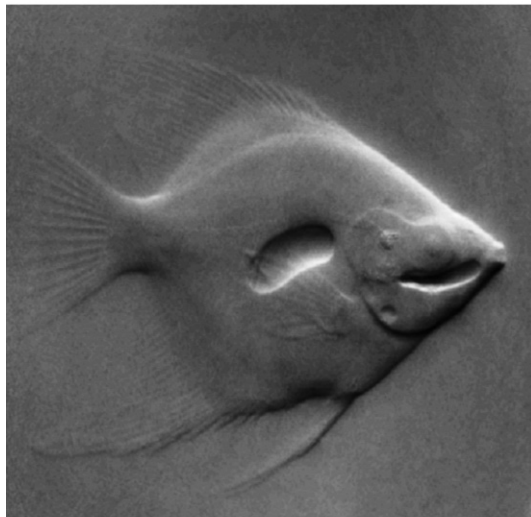
A number of samples have been imaged using the three-grating set-up described in Fig. 1b [7]. As an example for the phase contrast X-ray imaging, two images of a fish are shown in Fig. 6. Both the absorption contrast image and the phase image were acquired with the same X-ray dose. The phase image provided by the grating interferometer reveals a great amount of additional information and detail.

### 4. Conclusion and outlook

X-ray grating interferometry is a technique that can be applied to obtain images of the local phase gradients of large samples (several centimeters). It is possible to fabricate suitable gratings using standard lithography techniques. Future developments will focus on increasing the field of view and the photon energy. From the point of view of grating manufacturing it is feasible to produce gratings on larger silicon substrates than the currently used



Absorption contrast



Phase contrast

Fig. 6. X-ray images of a fish in conventional absorption contrast and phase contrast. The set-up was optimized for a photon energy of 17.5 keV. The field of view is 5 cm × 5 cm.

100 mm wafers. For typical applications in X-ray imaging the realistic samples may not only become larger but also thicker. Therefore, it is an important step to move towards higher energies. This would require even higher aspect ratio structures of the silicon beam splitter grating and the gold analyzer grating. Nickel causes a significantly stronger phase shift than silicon [6], therefore it may be an attractive alternative to reduce the required structure height for the beam splitter grating at higher photon energies. For the fabrication of the analyzer grating structures, there is no material available that has significantly higher attenuation than gold. The fabrication process described in Fig. 5, however, still has room for improvement in terms of the achievable aspect ratio.

#### Acknowledgement

This work was supported by the Swiss Commission for Technology and Innovation KTI/CTI under contact 7796.2 DCPN-NM.

#### References

- [1] R. Fitzgerald, *Phys. Today* 53 (7) (2000) 23–27.
- [2] A. Momose, *Opt. Express* 11 (2003) 2303–2314.
- [3] C. David, B. Nöhammer, H.H. Solak, E. Ziegler, *Appl. Phys. Lett.* 81 (17) (2002) 3287–3290.
- [4] T. Weitkamp, A. Diaz, C. David, F. Pfeiffer, M. Stampanoni, P. Cloetens, E. Ziegler, *Opt. Express* 13 (2005) 6296–6304.
- [5] F. Pfeiffer, T. Weitkamp, O. Bunk, C. David, *Nature Phys.* 2 (2006) 258–261.
- [6] B.L. Henke, E.M. Gullikson, J.C. Davis, *Atom. Data Nucl. Data* 54 (2) (1993) 181–342.
- [7] C. Kottler, F. Pfeiffer, O. Bunk, C. Grünzweig, J. Bruder, R. Kaufmann, L. Tlustos, H. Walt, I. Briod, C. David, *Phys. Stat. Sol. A*, accepted for publication.